

**Effect of H<sub>2</sub>S on the Corrosion Behavior of Pipeline Steels in Supercritical and Liquid CO<sub>2</sub> Environments**

Yoon-Seok Choi, Shokrollah Hassani, Thanh Nam Vu, Srdjan Nesic  
Institute for Corrosion and Multiphase Technology,  
Department of Chemical and Biomolecular Engineering, Ohio University  
342 West State Street  
Athens, OH 45701  
USA

Ahmad Zaki B Abas  
Petronas Research SDN. BHD, Selangor Darul Ehsan, Malaysia

**ABSTRACT**

The objective of the present study is to evaluate the corrosion properties of pipeline steels in CO<sub>2</sub>/H<sub>2</sub>S/H<sub>2</sub>O mixtures with different amounts of water (under-saturated and saturated) related to a natural gas transportation pipeline. Corrosion behavior of carbon steel, 1Cr steel and 3Cr steel was evaluated by using an autoclave with different combinations of CO<sub>2</sub> partial pressure and temperature (8 MPa/25°C and 12 MPa/80°C) with 200 ppm H<sub>2</sub>S. The corrosion rate of samples was determined by weight loss measurements. The surface morphology and the composition of the corrosion product layers were analyzed using surface analytical techniques (SEM and EDS). Results showed that the corrosion rate of materials in supercritical and liquid phase CO<sub>2</sub> saturated with water was very low (< 0.01 mm/y). However, adding 200 ppm of H<sub>2</sub>S to the supercritical and liquid CO<sub>2</sub> system caused mild corrosion (< 0.5 mm/y). Reducing water content to 100 ppm in the supercritical and liquid CO<sub>2</sub> systems with 200 ppm of H<sub>2</sub>S reduced the corrosion rate to less than 0.01 mm/y.

Key words: Supercritical/liquid CO<sub>2</sub>, CO<sub>2</sub> corrosion, H<sub>2</sub>S, carbon steel, low Cr steel

**INTRODUCTION**

Proven gas reserves in South East Asia are estimated at 5153 billion cubic metres (bcm), with Malaysia holding a 1047 bcm share. In the past, most of these gas fields were not economically viable due to the presence of large quantities of CO<sub>2</sub> (from 25% to 89%).<sup>1</sup> However, as the demand for energy rapidly grew, these resources become increasingly valuable. Produced gases from such fields are usually associated with potential high corrosion risks and resultant use of expensive Corrosion Resistant Alloys (CRAs). However, there is a need to better quantify the risk of corrosion associated with high pressure CO<sub>2</sub> environments in order to identify conditions in which mild steel may still be suitable when used with appropriate corrosion mitigation strategies. This has the potential to significantly reduce costs associated with use of CRAs for infrastructure construction.

Development of such high pressure CO<sub>2</sub> fields has to consider the presence of formation water which has the potential to contain a high concentration of corrosive species due to dissolved CO<sub>2</sub>. For offshore installations, it would be too costly to dry the gas stream or to remove CO<sub>2</sub> gas prior to transportation of hydrocarbon gas *via* pipelines. Due to the direct impact of the presence of formation water and high pressure CO<sub>2</sub> on the corrosion of pipeline steel, studies related to aqueous CO<sub>2</sub> corrosion at high CO<sub>2</sub> pressure have recently been conducted. It has been reported that the corrosion rate of carbon steel under high CO<sub>2</sub> pressure (liquid and supercritical CO<sub>2</sub>) without formation of protective FeCO<sub>3</sub> corrosion product layers is very high ( $\geq 20$  mm/y).<sup>2-6</sup> At certain conditions, the corrosion rate can decrease to low values (< 1 mm/y) after long-term exposures due to the formation of a protective layer of FeCO<sub>3</sub>.<sup>7-9</sup>

Usually, conventional CO<sub>2</sub> separation technologies remove CO<sub>2</sub> from natural gas at low pressure and release it to the atmosphere.<sup>10</sup> However, due to the large quantities of CO<sub>2</sub> present in the high pressure CO<sub>2</sub> gas fields, the CO<sub>2</sub> must be captured and transported to sequestration sites separately, which presents similar challenges as seen in CO<sub>2</sub> transmission related to carbon capture and storage (CCS). It has been acknowledged that dry supercritical and liquid CO<sub>2</sub> is not corrosive. However, recent studies have reported that the presence of trace impurities such as SO<sub>x</sub> and NO<sub>x</sub> can cause significant corrosion for carbon steel in supercritical and liquid CO<sub>2</sub> in the presence of small amounts of H<sub>2</sub>O (below the solubility limit).<sup>11-18</sup> Related to gas field development, it has recently been reported that there can be small amounts of H<sub>2</sub>S present in the high pressure CO<sub>2</sub> streams, whereas the effect on corrosion has thus far not been studied.

Figure 1 shows a schematic of a CO<sub>2</sub> transportation pipeline experiencing a temperature drop. At the inlet condition, the pressure is 12 MPa and temperature is 80°C. At this condition CO<sub>2</sub> is in the supercritical phase. Along the pipeline the temperature drops and consequently pressure drops and the CO<sub>2</sub> transitions from supercritical to liquid phase. Supercritical CO<sub>2</sub> at a pressure of 12 MPa and temperature of 80°C can dissolve 10,000 ppm of water.<sup>19</sup> However, liquid CO<sub>2</sub> at 8 MPa and 25°C can dissolve only 3,000 ppm water.<sup>19</sup> Therefore, temperature drop and consequently CO<sub>2</sub> phase transformation causes the formation of free water in the system.

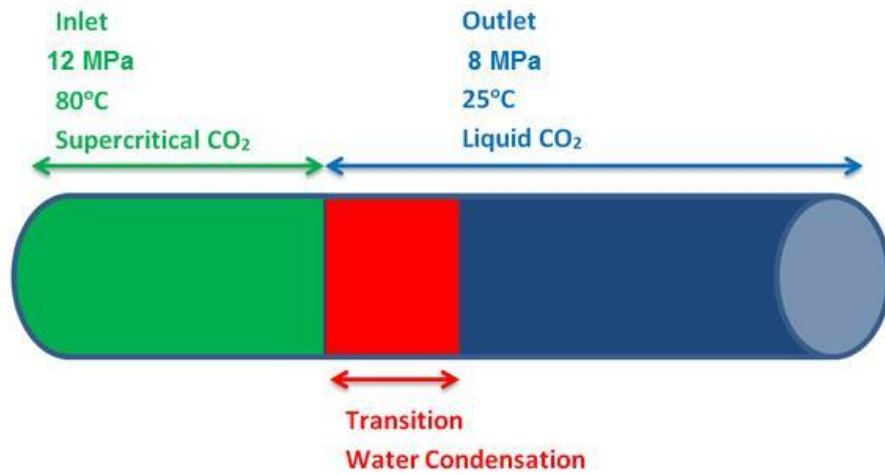


**Figure 1: Schematic of different parts of the pipeline with inlet and outlet conditions.**

Thus, the objective of the present study was to evaluate the corrosion performance of pipeline steels in supercritical and liquid CO<sub>2</sub> phases with and without temperature fluctuations and water condensation and also with and without H<sub>2</sub>S. Corrosion behavior of carbon steel, 1Cr steel and 3Cr steel was evaluated using an autoclave with different combinations of CO<sub>2</sub> partial pressure and temperature (8 MPa/25°C and 12 MPa/80°C) at a 200 ppm H<sub>2</sub>S concentration.

## EXPERIMENTAL PROCEDURE

The materials used in this work are as follow:

- UNS K03014 carbon steel, named CS
- UNS G41300-1Cr steel, named 1Cr
- UNS G41300-3Cr steel, named 3Cr

All materials were analyzed for chemical composition using Atomic Emission Spectroscopy (AES). Table 1 shows chemical compositions of the three materials used in the present study.

**Table 1**  
**Chemical compositions of materials used in the present study (wt.%, balance Fe).**

	C	Cr	Mn	P	S	Si	Cu	Ni	Mo	Al
CS	0.065	0.05	1.54	0.013	0.001	0.25	0.04	0.04	0.007	0.041
1Cr	0.3	0.85	0.91	0.015	0.008	0.29	---	---	---	---
3Cr	0.08	3.43	0.54	0.006	0.003	0.3	0.16	0.06	0.32	---

The specimens for the corrosion tests were machined to be rectangular with a size of 1.27 cm × 1.27 cm × 0.254 cm. A 5 mm diameter hole at one end serves to hang the samples from a sample stand with a non-metallic washer. The specimens were ground with 600-grit silicon carbide (SiC) paper, cleaned with isopropyl alcohol ( $i\text{-C}_3\text{H}_7\text{OH}$ ) in an ultrasonic bath, dried, and weighed using a balance with a precision of 0.1 mg.

The corrosion experiments were carried out in a 7.5-liter autoclave (UNS N10276). The electrolyte was a 1 wt.% NaCl solution. In the present study, the corrosion behavior of materials was evaluated in  $\text{CO}_2$ -rich phase (Figure 2), where samples were located in the  $\text{CO}_2$  phase. Water content at the bottom of the autoclave was varied in correspondence with the water concentration in the  $\text{CO}_2$  phase. Once sealed, the autoclave temperature was adjusted. Then, a mixture of  $\text{CO}_2$  and  $\text{H}_2\text{S}$  was directly injected into the autoclave to the desired  $\text{H}_2\text{S}$  concentration (200 ppm). Finally, high pressure  $\text{CO}_2$  was added to the autoclave with a gas booster pump to the desired working pressure.

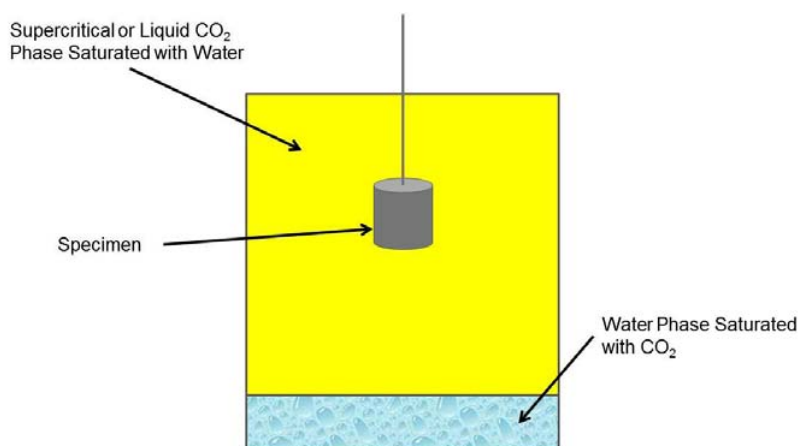


**Figure 2: Schematic of specimen location in the autoclave.**

The corrosion rates were determined from the weight-loss method at the end of the test. In each test, two specimens were simultaneously exposed to the corrosive environment in order to obtain an averaged corrosion rate. The specimens were removed and cleaned for 5 min in Clarke solution (20 g antimony trioxide + 50 g stannous chloride and hydrochloric acid to make 1000 ml). The specimens were then rinsed in distilled water, dried and weighed to 0.1 mg. The average corrosion rate during the test period can be calculated by the following equation:<sup>20</sup>

$$\text{Corrosionrate (mm/y)} = \frac{8.76 \times 10^4 (\text{mm} \cdot \text{hour/cm} \cdot \text{year}) \times \text{weightloss(g)}}{\text{area (cm}^2\text{)} \times \text{density(g/cm}^3\text{)} \times \text{time(hour)}} \quad (1)$$

The morphology and compositions of corrosion products were analyzed using scanning electron microscopy (SEM) and energy dispersive X-ray spectroscopy (EDS).

### Corrosion in CO<sub>2</sub> Phase without Water Condensation

Table 2 shows the test matrix for corrosion of materials in supercritical/liquid CO<sub>2</sub> phases with different amounts of water and H<sub>2</sub>S. For the water-saturated CO<sub>2</sub> condition, 10 g of 1 wt.% NaCl solution was added to the autoclave in order to ensure saturation. Tests with 100 ppm of water represent under-saturated conditions.

**Table 2**  
**Test conditions for corrosion study in the CO<sub>2</sub>-rich phase without condensation**

	Material	pCO <sub>2</sub> (MPa)	H <sub>2</sub> S (ppm)	Temperature (°C)	Duration (hours)	Water content
H <sub>2</sub> O saturated	CS	12	0	25	24	saturated
	CS	12	0	80	24	saturated
	1Cr	12	0	25	24	saturated
	1Cr	12	0	80	24	saturated
H <sub>2</sub> S & H <sub>2</sub> O saturated	CS	12	200	80	48	saturated
	1Cr	12	200	80	48	saturated
	3Cr	12	200	80	48	saturated
	CS	8	200	25	48	saturated
	1Cr	8	200	25	48	saturated
	3Cr	8	200	25	48	saturated
H <sub>2</sub> S & H <sub>2</sub> O under-saturated	CS	12	200	25	24	100 ppm
	CS	12	200	80	24	100 ppm
	1Cr	12	200	25	24	100 ppm
	1Cr	12	200	80	24	100 ppm

\*ppm = ppm<sub>v</sub>

### Corrosion in CO<sub>2</sub> phase with water condensation

Figure 3 shows experimental procedures for evaluating dewing corrosion behavior of materials at high pCO<sub>2</sub> conditions. Initially, 10 g of 1 wt.% NaCl solution was added to the autoclave in order to ensure saturation. The decrease in temperature during experiments will cause water condensation on the specimen surface and provide a condition for dissolving CO<sub>2</sub> and H<sub>2</sub>S therein. It is important to note that only one cycle of dewing was simulated experimentally. Table 3 shows the test matrix for the dewing corrosion study.

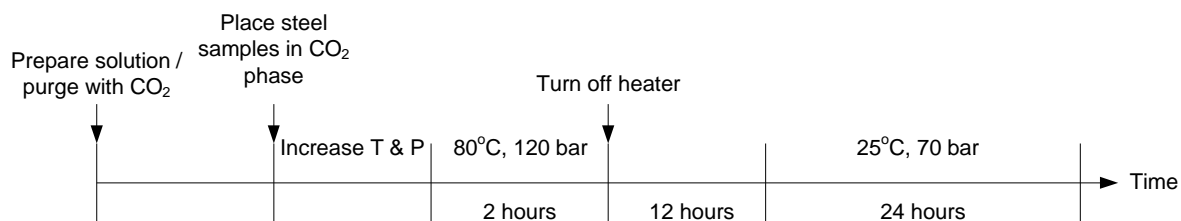


**Figure 3: Experimental procedures for evaluating the dewing corrosion behavior of materials in high pCO<sub>2</sub> environments with H<sub>2</sub>S.**

**Table 3  
Test conditions for dewing corrosion study**

	Material	pCO <sub>2</sub> (MPa)	H <sub>2</sub> S (ppm)	Temperature (°C)	Water content
Dewing	CS	12	0	80 → 25	saturated
	1Cr	12	0	80 → 25	saturated
	3Cr	12	0	80 → 25	saturated
	CS	12	200	80 → 25	saturated
	1Cr	12	200	80 → 25	saturated
	3Cr	12	200	80 → 25	saturated

\*ppm = ppmv

## RESULTS AND DISCUSSION

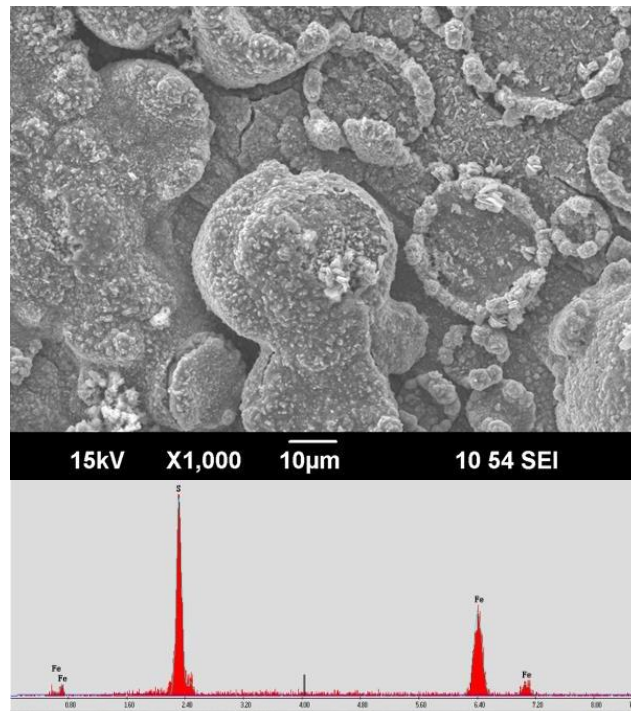
### Corrosion in CO<sub>2</sub> phase without water condensation

Table 4 shows the summary of corrosion rate data of three different steels in the supercritical CO<sub>2</sub> phase (inlet condition) and liquid CO<sub>2</sub> phase (outlet condition) with and without H<sub>2</sub>S. Experimental data shows that corrosion rate in supercritical and liquid CO<sub>2</sub> phases saturated with water is very low (< 0.01 mm/y), consistent with previous results.<sup>11,12,21,22</sup> However, adding H<sub>2</sub>S to the supercritical and liquid CO<sub>2</sub> systems leads to corrosion. Furthermore, reducing water content to 100 ppm in supercritical and liquid CO<sub>2</sub> systems with 200 ppm H<sub>2</sub>S reduced the corrosion rate to less than 0.01 mm/yr.

Figure 4 and Figure 5 show SEM images and EDS spectra of the corroded CS sample surface and cross-section, exposed to water-saturated supercritical CO<sub>2</sub> (12 MPa, 80°C) with 200 ppm of H<sub>2</sub>S. As shown in Figure 4, the surface was covered by corrosion products that consisted of Fe and S. This indicates the formation of FeS on the steel surface under this condition. Furthermore, it can be seen from Figure 5 that it has a bilayer structure; an outer thin FeS layer and a thick/continuous inner FeCO<sub>3</sub> layer. A similar morphology was observed for 1Cr steel. Figure 6 shows the SEM image and EDS spectra of the corroded surface of 3Cr steel after exposure to water-saturated supercritical CO<sub>2</sub> (12 MPa, 80°C) with 200 ppm of H<sub>2</sub>S. It can be seen that the surface was covered by a thin layer of sulfur-containing corrosion products. Note that the polishing marks are still visible, indicating that the corrosion of this material was minimal, compare to CS and 1Cr steel.

**Table 4**  
**Summary of corrosion rate data of three different steels in CO<sub>2</sub> phase**

	Material	pCO <sub>2</sub> (MPa)	H <sub>2</sub> S (ppm)	Temp. (°C)	Water content	Corrosion Rate (mm/y)
<b>H<sub>2</sub>O saturated</b>	CS	12	---	25	saturated	< 0.01
	CS	12	---	80	saturated	< 0.01
	1Cr	12	---	25	saturated	< 0.01
	1Cr	12	---	80	saturated	< 0.01
<b>H<sub>2</sub>S &amp; H<sub>2</sub>O saturated</b>	CS	12	200	80	saturated	0.41
	1Cr	12	200	80	saturated	0.44
	3Cr	12	200	80	saturated	0.05
	CS	8	200	25	saturated	0.07
	1Cr	8	200	25	saturated	0.13
	3Cr	8	200	25	saturated	0.14
<b>H<sub>2</sub>S &amp; H<sub>2</sub>O under-saturated</b>	CS	12	200	25	100 ppm	< 0.01
	CS	12	200	80	100 ppm	< 0.01
	1Cr	12	200	25	100 ppm	< 0.01
	1Cr	12	200	80	100 ppm	< 0.01



**Figure 4: SEM image and EDS spectra of the surface of CS after exposure to water-saturated supercritical CO<sub>2</sub> (12 MPa, 80°C) with 200 ppm of H<sub>2</sub>S.**

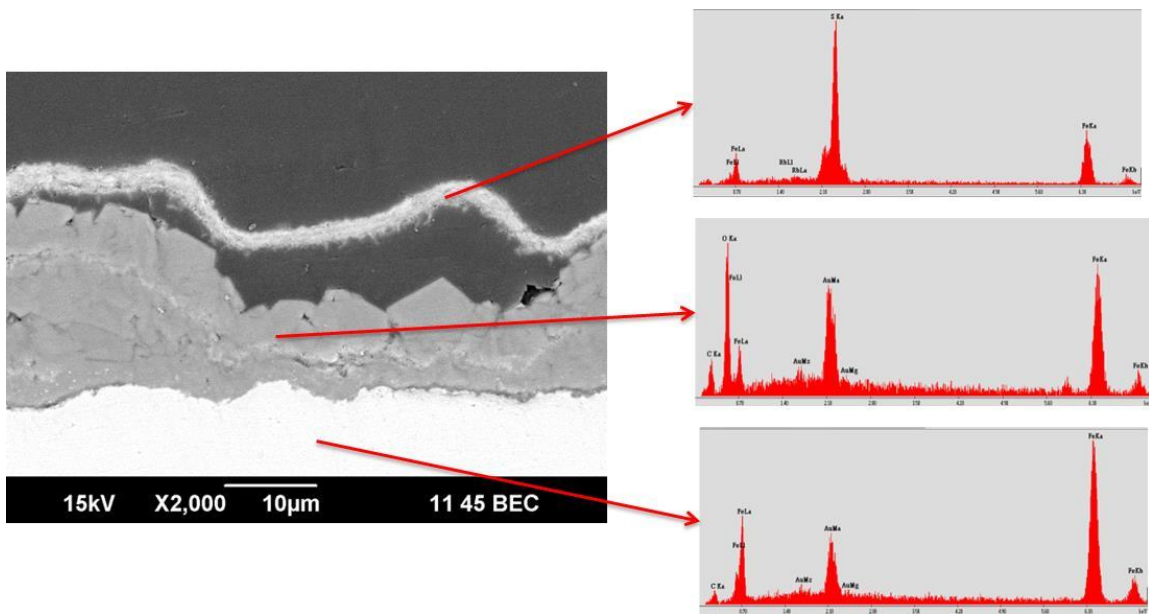


Figure 5: SEM image and EDS spectra of the cross-section of CS after exposing to water-saturated supercritical CO<sub>2</sub> (12 MPa, 80°C) with 200 ppm of H<sub>2</sub>S

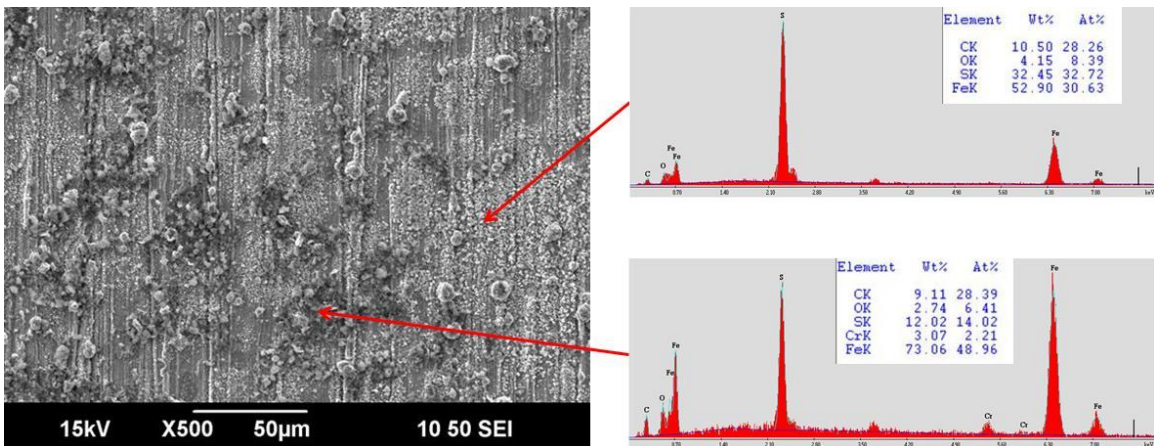
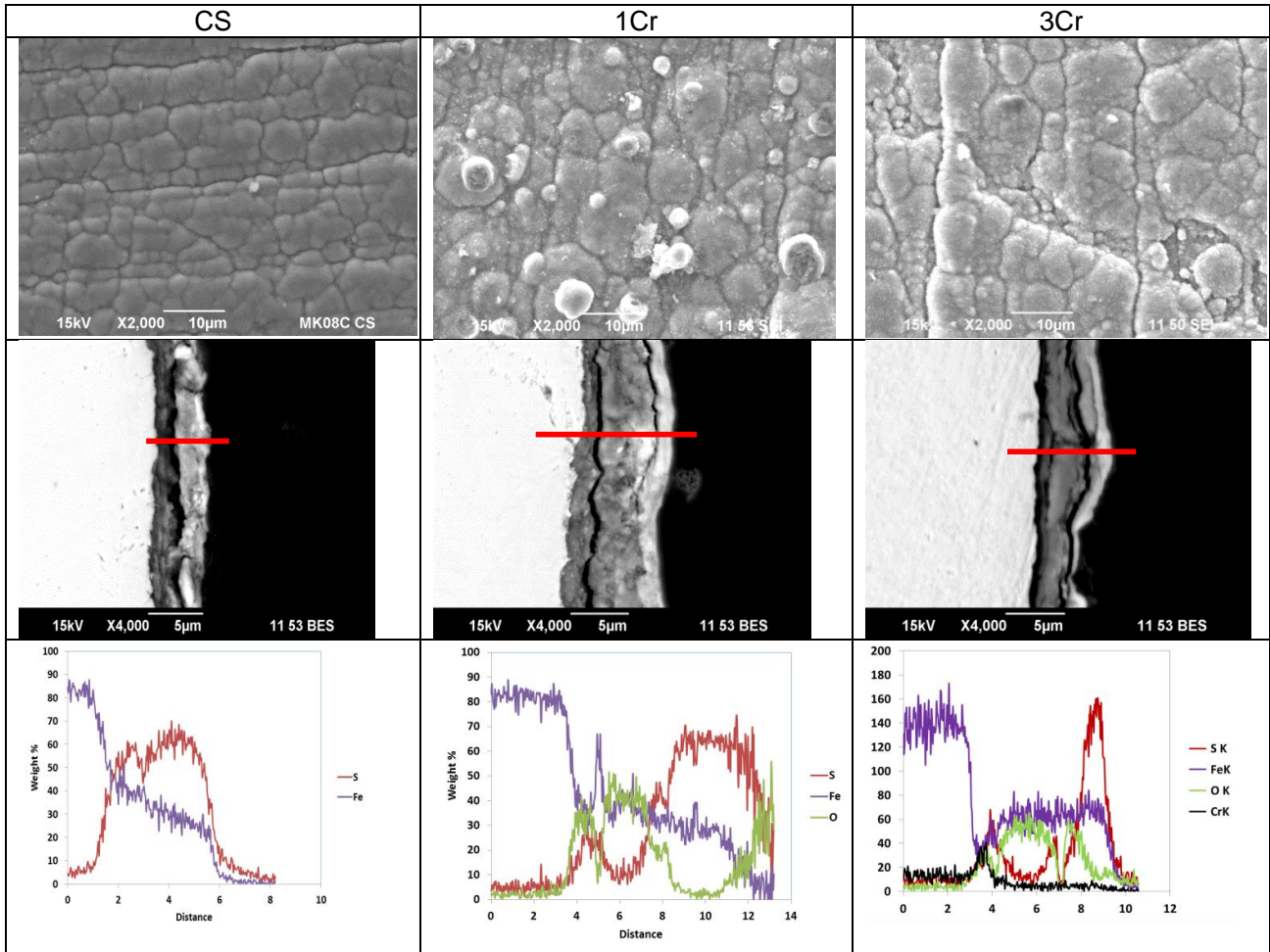


Figure 6: SEM image and EDS spectra of the surface of 3Cr steel after exposing to water-saturated supercritical CO<sub>2</sub> (12 MPa, 80°C) with 200 ppm of H<sub>2</sub>S.

Figure 7 shows SEM images and EDS line scanning results of the corroded samples (CS, 1Cr and 3Cr steels) for their surfaces and in cross-section after exposure to water-saturated supercritical CO<sub>2</sub> (8 MPa, 25°C) with 200 ppm of H<sub>2</sub>S. SEM surface analysis shows a similar morphology for corrosion products for all three steels. EDS elemental analysis shows that the corrosion product layer is mostly FeS. EDS line scanning also shows that for 3Cr steel there is a chromium rich layer close to the metal surface and underneath the FeS layer. This chromium rich layer reduces the adherence of corrosion products to the metal surface and, consequently, reduces the protectiveness of the corrosion product layer and increases the corrosion rate. It is interesting to note that under this low temperature condition (25°C), FeCO<sub>3</sub> was not observed on the surface of the CS and 1Cr steel.



**Figure 7: SEM and EDS analyses of three different steels after corrosion experiments in liquid CO<sub>2</sub> phase saturated with H<sub>2</sub>O at 8 MPa, 25°C and also containing 200 ppm of H<sub>2</sub>S.**

As shown in above results, adding 200 ppm of H<sub>2</sub>S increased the corrosion rate of materials in the water-saturated CO<sub>2</sub> phase. This indicates that H<sub>2</sub>S can react with materials in the presence of a small amount of water. A lower surface energy condition on the steel can result in development of nucleation sites for the formation of water droplets saturated with H<sub>2</sub>S and CO<sub>2</sub>, which in turn leads to formation of both iron carbonate and iron sulfide on the steel surface at high temperature (80°C). Increasing the temperature from 25 to 80°C increased the corrosion rate almost 5 times because of increasing the saturated water content in the CO<sub>2</sub> phase (*i.e.*, from 3000 to 10000 ppm of water in the CO<sub>2</sub> phase)<sup>19</sup> and also accelerating the rate of chemical and electrochemical reactions.

Figure 8 shows the surface appearance of the CS and 1Cr steel samples exposed to the supercritical CO<sub>2</sub> phase (12 MPa, 80°C) with 100 ppm of water and 200 ppm of H<sub>2</sub>S for 24 hours. No visible signs of corrosion were observed on samples, *i.e.*, the surfaces appeared shiny and devoid of any type of corrosion products.

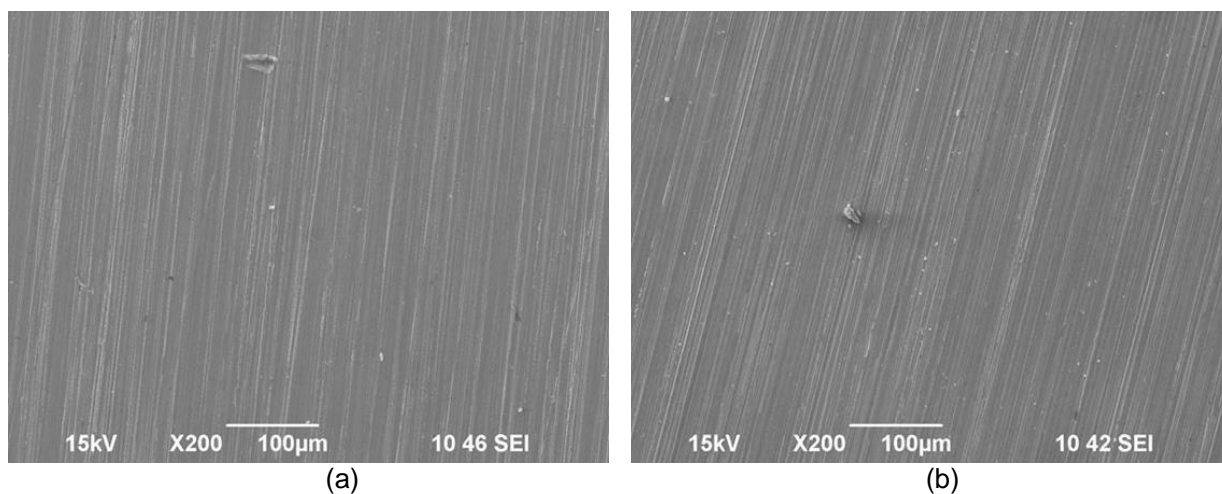


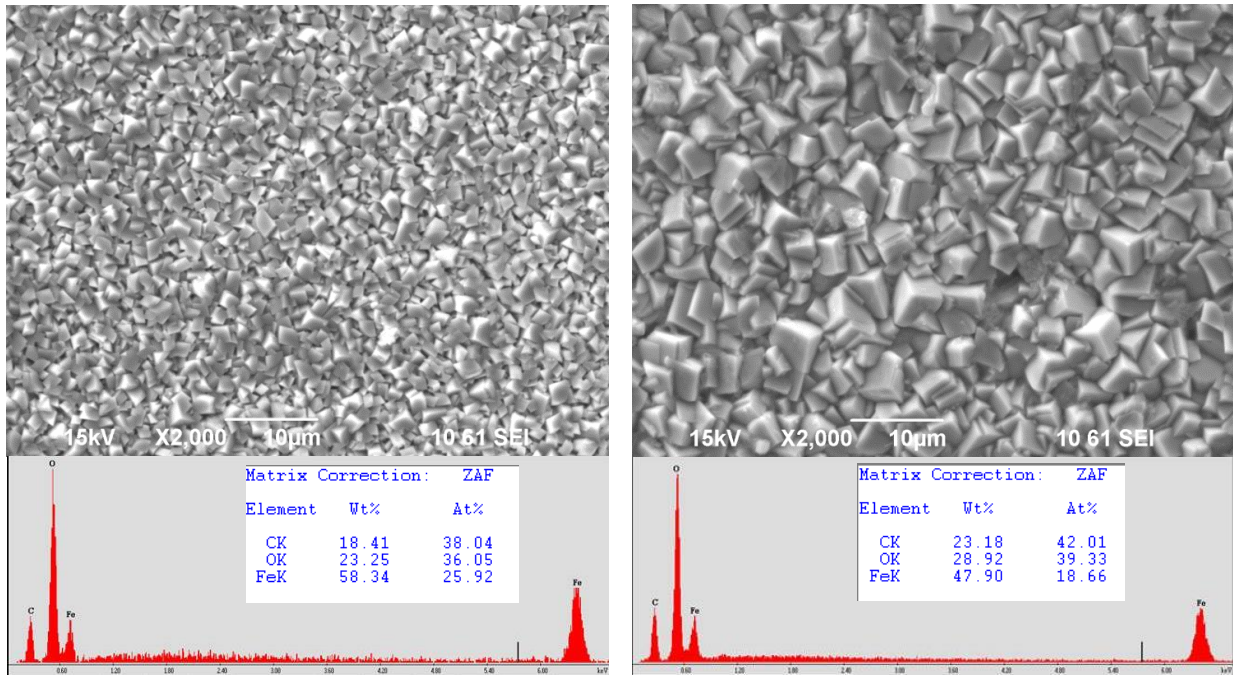
**Figure 8: SEM images of the sample surface exposed to the supercritical CO<sub>2</sub> phase (12 MPa, 80°C) with 100 ppm of water and 200 ppm of H<sub>2</sub>S for 24 hours: (a) CS, (b) 1Cr steel.**

### **Corrosion in CO<sub>2</sub> phase with water condensation (Dewing Corrosion)**

Temperature fluctuations in CO<sub>2</sub> transportation pipelines causes phase transitions and consequent water condensation (Figure 1). A summary of corrosion experimental data under these conditions is shown in Table 5. Without any condensation and dewing in the system, no corrosion happens without H<sub>2</sub>S (Table 4). However, under dewing conditions, corrosion happens both in pure CO<sub>2</sub> and CO<sub>2</sub>/H<sub>2</sub>S systems. SEM and EDS surface analysis of steel after dewing corrosion of CS, 1Cr and 3Cr steels in pure CO<sub>2</sub> and CO<sub>2</sub>/200 ppm H<sub>2</sub>S systems are shown in Figure 9 and Figure 10, respectively. The corrosion products in the pure CO<sub>2</sub> system are mainly FeCO<sub>3</sub>, whereas in the CO<sub>2</sub>/H<sub>2</sub>S system, the presence of FeS is dominant.

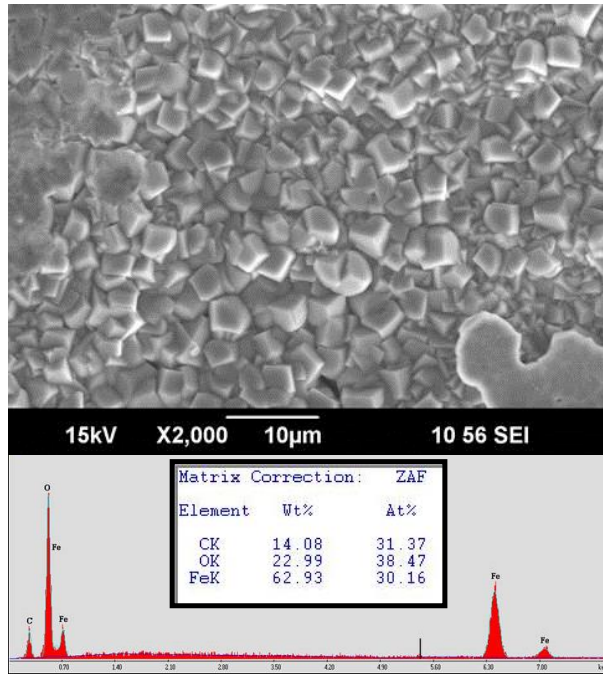
**Table 5  
Summary of corrosion rate data of three different steels in CO<sub>2</sub> phase.**

	Material	pCO <sub>2</sub> (MPa)	H <sub>2</sub> S (ppm)	Temperature (°C)	Water content	Corrosion rate (mm/y)
Dewing	CS	12	0	80 → 25	saturated	0.15
	1Cr	12	0	80 → 25	saturated	0.12
	3Cr	12	0	80 → 25	saturated	0.07
	CS	12	200	80 → 25	saturated	0.82
	1Cr	12	200	80 → 25	saturated	0.76
	3Cr	12	200	80 → 25	saturated	0.42



(a)

(b)



(c)

**Figure 9: SEM and EDS surface analysis of the sample surface after corrosion experiment in CO<sub>2</sub> phase experiencing temperature fluctuation without H<sub>2</sub>S: (a) CS, (b) 1Cr steel, (c) 3Cr steel.**

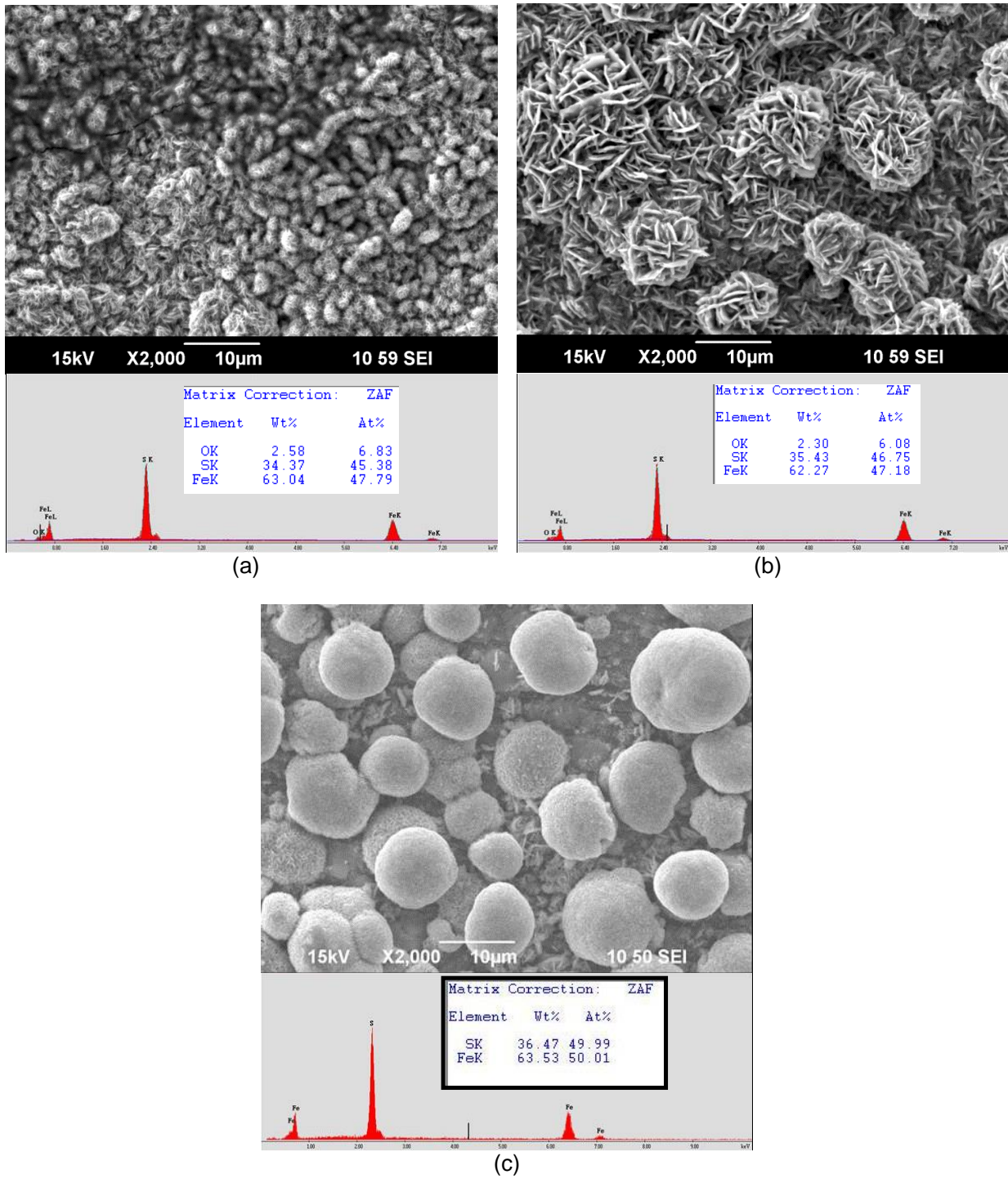


**Figure 10: SEM and EDS surface analysis of the sample surface after corrosion experiment in  $\text{CO}_2$  phase experiencing temperature fluctuation with 200 ppm of  $\text{H}_2\text{S}$ : (a) CS, (b) 1Cr steel, (c) 3Cr steel.**

## CONCLUSIONS

The corrosion properties of pipeline steels in CO<sub>2</sub>/H<sub>2</sub>S/H<sub>2</sub>O mixtures with different amounts of water (both saturated and under-saturated) were investigated by weight loss measurements and surface analysis techniques. The following conclusions are drawn:

- There was no significant corrosion attack in the supercritical and liquid CO<sub>2</sub> phases in the presence of water (both saturated and under-saturated).
- The addition of 200 ppm H<sub>2</sub>S in the CO<sub>2</sub> phase dramatically increased the corrosion rate of all tested materials (CS, 1Cr and 3Cr steels) when CO<sub>2</sub> was saturated with water.
- Under dewing conditions, corrosion happens both in pure CO<sub>2</sub> and CO<sub>2</sub>/H<sub>2</sub>S systems due to the formation of water droplets on the sample surface.
- 3Cr steel showed better corrosion resistance for the tested conditions compared with CS and 1Cr steel.

## REFERENCES

1. J. Veron, "An overview of the non-developed gas reserves in Southeast Asia," *PetroMin* (2007): p. 22.
2. M.F. Mohamed, A. Mohammed Nor, M.F. Suhor, M. Singer, Y.S. Choi and S. Nestic, "Water Chemistry for Corrosion Prediction in High-pressure CO<sub>2</sub> Environments," CORROSION 2011, paper no. 11375 (Houston, TX: NACE, 2011).
3. A. Mohammed Nor, M.F. Suhor, M.F. Mohamed, M. Singer and S. Nestic, "Corrosion of Carbon Steel in High CO<sub>2</sub> Environment: Flow Effect," CORROSION 2011, paper no. 11245 (Houston, TX: NACE, 2011).
4. Y. Zhang, X. Pang, S. Qu, X. Li, K. Gao, "The Relationship Between Fracture Toughness of CO<sub>2</sub> Corrosion Scale and Corrosion Rate of X65 Pipeline Steel Under Supercritical CO<sub>2</sub> Condition," *International Journal of Greenhouse Gas Control* 5 (2011): p. 1643.
5. A. Mohammad Nor, M.F. Suhor, M.F. Mohamed, M. Singer, S. Nestic, "Corrosion of Carbon Steel in High CO<sub>2</sub> Containing Environments: the Effect of High Flow Rate," CORROSION 2012, paper no. 0001683 (Houston, TX: NACE, 2012).
6. Y.S. Choi, D. Young, S. Nestic, L.G.S. Gray, "Wellbore Integrity and Corrosion of Carbon Steel in CO<sub>2</sub> Geologic Storage Environments: A Literature Review," *International Journal of Greenhouse Gas Control* 16S (2013): p. S70.
7. M.F. Suhor, M.F. Mohamed, A. Mohammad Nor, M. Singer, S. Nestic, "Corrosion of Mild Steel in High CO<sub>2</sub> Environment: Effect of the FeCO<sub>3</sub> Layer," CORROSION 2012, paper no. 0001434 (Houston, TX: NACE, 2012).
8. Y. Zhang, X. Pang, S. Qu, X. Li, K. Gao, "Discussion of the CO<sub>2</sub> Corrosion Mechanism Between Low Partial Pressure and Supercritical Condition," *Corrosion Science* 59 (2012): p. 186.
9. Y.S. Choi, F. Farelles, S. Nestic, A.A.O. Magalhães, C. de Azevedo Andrade, "Corrosion Behavior of Deep Water Oil Production Tubing Material under Supercritical CO<sub>2</sub> Environment: Part 1—Effect of Pressure and Temperature," *Corrosion* 70 (2014): p. 38.
10. A. Hart, N. Gnanendran, "Cryogenic CO<sub>2</sub> Capture in Natural Gas," *Energy Procedia* 1 (2009): p. 697.
11. Y.S. Choi, S. Nestic, D. Young, "Effect of Impurities on the Corrosion Behavior of CO<sub>2</sub> Transmission Pipeline Steel in Supercritical CO<sub>2</sub>-Water Environments," *Environmental Science and Technology* 44 (2010): p. 9233.
12. Y.S. Choi, S. Nestic, "Effect of Water Content on the Corrosion Behavior of Carbon Steel in Supercritical CO<sub>2</sub> Phase with Impurities," CORROSION 2011, paper no. 11377 (Houston, TX: NACE, 2011).
13. Y. Xiang, Z. Wang, C. Xu, C. Zhou, Z. Li, W. Ni, "Impact of SO<sub>2</sub> Concentration of the Corrosion Rate of X70 Steel and Iron in Water-Saturated Supercritical CO<sub>2</sub> Mixed with SO<sub>2</sub>," *J. of Supercritical Fluids* 58 (2011): p. 286.
14. A.S. Ruhl, A. Kranzmann, "Corrosion in Supercritical CO<sub>2</sub> by Diffusion of Flue Gas Acids and Water," *J. of Supercritical Fluids* 68 (2012): p. 81.

15. A. Dugstad, M. Halseid, B. Morland, "Effect of SO<sub>2</sub> and NO<sub>2</sub> on Corrosion and Solid Formation in Dense Phase CO<sub>2</sub> Pipelines," *Energy Procedia* 37 (2013): p. 2877.
16. F. Farelas, Y.S. Choi, S. Nestic, "Corrosion Behavior of API 5L X65 Carbon Steel under Supercritical and Liquid CO<sub>2</sub> Phases in the Presence of H<sub>2</sub>O and SO<sub>2</sub>," *Corrosion* 69 (2013): p. 243.
17. O. Yevtushenko, D. Bettge, S. Bohraus, R. Bäßler, A. Pfennig, A. Kranzmann, "Corrosion Behavior of Steels for CO<sub>2</sub> Injection," *Process Safety and Environmental Protection* 92 (2014): p. 108.
18. S. Sim, I.S. Cole, Y.S. Choi, N. Birbilis, "A Review of the Protection Strategies against Internal Corrosion for the Safe Transport of Supercritical CO<sub>2</sub> via Steel Pipelines for CCS Purposes," *International Journal of Greenhouse Gas Control* 29 (2014): p. 185.
19. Y. S. Choi, S. Nestic, "Determining the Corrosive Potential of CO<sub>2</sub> Transport Pipeline in High pCO<sub>2</sub>-Water Environments," *International Journal of Greenhouse Gas Control* 5 (2011): p. 788.
20. ASTM Standard G31, "Standard Practice for Laboratory Immersion Corrosion Testing of Metals," in Annual Book of ASTM Standards, vol. 03. 02 (West Conshohocken, PA: ASTM International, 1994)
21. S. Sim, F. Bocher, I.S. Cole, X.B. Chen, N. Birbilis, "Investigating the Effect of Water Content in Supercritical CO<sub>2</sub> as Relevant to the Corrosion of Carbon Capture and Storage Pipelines," *Corrosion* 70 (2014): p. 185.
22. Y. Hua, R. Barker, A. Neville, "Effect of Temperature on the Critical Water Content for General and Localised Corrosion of X65 Carbon Steel in the Transport of Supercritical CO<sub>2</sub>," *International Journal of Greenhouse Gas Control* 31 (2014): p. 48.